2013 ISES Solar World Congress

Cloud cover forecasting from METEOSAT data

Francisco Javier Batlles[a],*, Joaquín Alonso[b], Gabriel López[c]

[a]Dpto. Física Aplicada, Universidad de Almería, 04120 Almería, Spain
[b]CIESOL, Joint Centre Universidad de Almería-CIEMAT, 04120 Almería, Spain
[c]Escuela Técnica Superior de Ingeniería, Universidad de Huelva, 21819 Palos de la Frontera, Spain

Abstract

Solar thermoelectric energy has a great potential as an energy supplier in many countries around the world. Since clouds are the main cause to solar radiation blocking, short term cloud forecasting can help power plant operation and therefore improve benefits. Therefore, cloud detection, classification and motion vector determination are key to forecast sun obstruction by clouds. Geostationary satellites provide cloud information covering wide areas, allowing cloud forecast to be performed for several hours in advance. Herein, the methodology developed and tested in this study is based on multispectral tests and binary cross correlations followed by coherence and quality control tests over resulting motion vectors. The following methodology utilizes Meteosat Second Generation imagery. In addition, pyrheliometric data and a whole-sky camera have also been used to test the methodology results . Cloud classification in terms of opacity and height of cloud top is also performed. Results show an agreement above 90% between satellite detected and observed cloud cover for cloudless and overcast situations and over 75% for partially cloudy skies, whereas around the 86% of the motion vectors are well determined. This work represents the starting point for addressing the prediction of solar radiation to short time using satellite imagery.

* Corresponding author. Tel.: +34-950215914; fax: +34-950215477.
E-mail address: fbatlles@ual.es.

1. Introduction

Solar power plants could play an important role in the next few decades when they become profitable. A possibility to improve solar power plant performance is by forecasting the short-term solar irradiation profile, allowing operators to take decisions on the operation mode, thus optimizing the use of storage systems. Cloud coverage is the most attenuating factor of beam solar radiation. Predicting when and how long the sun will be covered by clouds would improve solar plant operation. Thus, cloud detection, cloud classification and cloud motion determination are suggested as the main sources of information for solar plant operation improvement by anticipating the power or thermal storage use.

Cloud cover has been studied, using satellite images. Janjai et al. (2009) [1] derived global hourly solar radiation using the Geosynchronous Meteorological Satellite 5 (GMS-5) satellite. More recently, Şencal (2010) [2] used remote sensing and Artificial Neural Networks (ANNs) to predict global solar radiation without any meteorological data and with a relatively good agreement between measures and predicted values. Hourly global radiation was estimated by Lu et al. (2011) [3], using images of the visible and infrared bands of the Multi-purpose Transport Satellite (MTSAT) and the Geostationary Operational Environmental Satellite (GOES).

Short-term solar radiation forecast is based on real-time processing of the satellite images instead of a long-time series analysis. To study cloud motion, it is first necessary to classify cloudy and clear pixels on the images. Several studies utilize multispectral analysis to classify cloudy and clear pixels [4,5,6,7]. Other methods have been developed to classify the pixels, many of them based on statistical analysis. Thiermann and Ruprecht (1992) [8] tried a single infrared channel detection over sea pixels. Amato et al. (2008) [9] showed that spectral signature of each pixel contains information on the physical characteristics of the land or cloud. Ricciardelli et al. (2008) [10] combined physical, statistical and temporal techniques for cloud detection to classify pixels as cloudy or cloudless.

Multispectral analysis is the most known and developed method to detect clouds. In this work, new thresholds for infrared and visible tests based on monthly averaged values are proposed. Synthetic images of mean minimum surface temperature and surface albedo are used to determine the thresholds, following the methodology by Moussu et al. (1989) [11]. Cloud classification is done in terms of both cloud top height and cloud opacity. Cloud top height classifies clouds in low, medium and high. Monthly tropospheric air temperature-height correlation has been done based on sounder data. Nieman et al. (1993) [12] mentions this technique applied to opaque clouds. Additionally, a radiometric study has been done to classify clouds in term of opacity using Meteosat Second Generation (MSG) imagery.

In this work, cloud motion vectors are used for solar radiation short-term forecast. Binary cross-correlation is commonly used for cloud tracking and is utilized in this work, applied to the previously detected cloudy pixels [13]. Also, the maximum cross-correlation method is used, which has proven to be a good approach [13,14,15,16]. Once the image is segmented by sectors and by heights, each sub-matrix is used as a tracer for the tracking correlation. Quality control is performed over the resulting vectors in order to reject incoherent and erroneously detected motions. This paper shows a methodology to determine these three sources of information for short-term prediction of cloudiness. Therefore, this methodology is the first and fundamental step to predict solar radiation in a short time using this type of images.

2. Materials and methods

2.1 Data collection

The following methodology utilizes MSG imagery for the short term cloud forecast. Radiometric calibration constants are also needed. These constants are included in the MSG images. A 121x161 pixel raster image, for every of the five used channels, centered at the University of Almería, is used. This image size covers a ~500x500 km^2 image, large enough for 1 hour forecast as the fastest clouds could be detected before they reach the midpoint. Pyrheliometric data and a whole-sky camera TSI-880 (placed at the University of Almería) have also been used to test the methodology results.

2.2 Cloud detection test

The first step before is to convert gray levels of the raster image into reflectances (for short-wave channels) and temperatures (for long-wave channels). The relation between radiance and temperature used in this work is based on Plank's law with the expression shown in the Equation (1):

$$T = \frac{A}{\log(1 + L^B) + C} \qquad (1)$$

where T stands for the temperature in Kelvin and A, B and C are constants fitted from [17].

Reflectance and temperature pixel values, or an algebraic combination of them are compared with different thresholds to tell cloudy from cloudless pixels.

2.2.1 Literature threshold tests

Four tests from literature have been used in this work unchanged. A snow detection test has been used prior to the other test to avoid misclassification of bright cold snowy cloud free pixels, Derrien and Le Gléau (2010) [18]. Infrared - visible channel ratio test [19], emissivity difference test [5, 18] and spatial texture test [20], have been used according to their references in order to improve cloud detection.

2.2.2 Monthly synthetic raster threshold tests

Two common threshold tests have been improved by replacing spatially constant threshold values for synthetic raster images with specific monthly threshold values for each pixel.

- *Visible reflectance threshold test*.

Channel centered at 0.6 μm has been taken for land pixels whereas channel centered at 0.8 μm has been taken for sea pixels as many authors recommend [18, 19, 41]. Assuming that clouds have a wide spectrum of reflectance values and that surface albedo has a rather constant monthly reflectance, the most repeated value should be the surface albedo. Thus, mode from reasonable albedo interval ([0.1,0.4] for land and [0.0,0.3] for sea) is taken as pixel surface albedo. Figure 1 shows the surface albedo raster for the month of December.
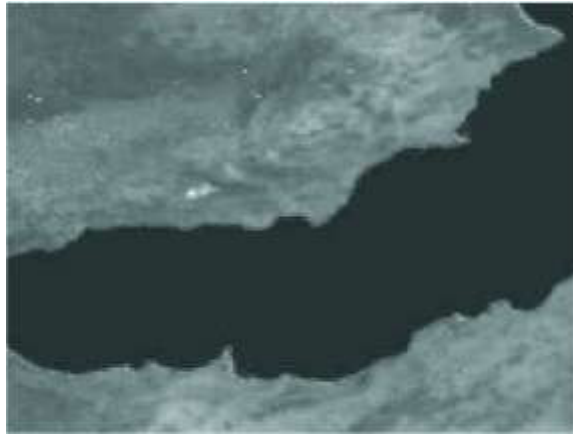
Fig. 1. Synthetic raster of reference surface albedo for the month of December

If reflectance is higher than surface albedo plus an offset (set to 0:08 during this research), a pixel is flagged as cloudy.

- *Infrared temperature threshold test.*

Two sources have been used to elaborate monthly synthetic rasters of surface temperature. The one for sea pixels is monthly minimum sea surface minimum temperature from the Satellite Application Facility on support to Nowcasting (SAFNWC) database. The one for land pixels is the monthly mean minimum temperature from the Spanish Meteorological State Agency (AEMET) stations. A cubic interpolation and a nearest neighbor extrapolation have been done to fill pixel without values (i.e. missing values, gaps). The 10.8 μm channel temperature value is compared with the monthly mean minimum surface temperature reference of each pixel, T_{min}. If temperature is lower than the minimum value minus an offset, pixel is flagged as cloudy. Offset values can be found in Derrien et al. (1993) [6].

2.3 Opaque cloud tagging

It is assumed that opaque clouds would reflect more solar radiation than thin clouds; so they should have a higher value on visible channels reflectance. 247 pyrheliometric data have been split into two groups: above 400 W m^{-2} (66.7%) and below 400 W m^{-2} (33.3%). Every cloud detection test, some linear combination of them, an opaque cloud test suggested by Derrien and Le Gléau (2010) [18] and cloud top height layer have been compared against each other to find the best way to tag cloudy pixels as opaque ones, potentially able to reduce direct irradiance below 400 W m^{-2}.

2.4 Cloud motion

Pixel thermal information could be linked with cloud top temperature and then with cloud top height, assuming thermal equilibrium with its surroundings and comparing its top temperature with air measurements at different altitudes. Sounding air measurements from a weather station in the city of Murcia, close to Almería, have been taken from The University of Wyoming worldwide sounding database to fit a monthly second-order polynomial curve of vertical temperature-height profile [21].

Mean data deviation is 1.0 km and maximum deviation is 1.3 km for the month of April. Based on this result, cloud layers are classified into low, medium and high [22].

Raster image is further divided into five horizontal sectors defined around the place of study. Four rectangular sectors are obtained dividing raster image along its two bisections. The fifth sector is the same shape and size as the previous ones, but centered at the center of the raster. Thus, 15 binary matrices (cloud/cloud-free pixel) are generated for one raster image.

2.5 Raster segmentation and binary cross correlation

Three consecutive raster images are used for cloud tracking (image 1, 2 and 3) and one motion vector is determined for each sector and each height. For each sector and height, a maximum cross correlation is performed between images 1 and 2; v_{1-2} vector is obtained as the distance between centers of matching windows, 2 and 3 (v_{2-3}); and 1 and 3 (v_{1-3}). Assuming a steady motion, v_{1-2} and v_{2-3} vectors should be of equal magnitude and phase, and both equal to half of v_{1-3} vector.

To avoid multilayer cloud cover affecting cross correlation, another cross correlation is performed over the non-height-divided image (5 more track vectors, one for each sector). Moreover, to avoid outgoing clouds affecting individual cross correlation, the entire raster image is also correlated (3+1 more track vectors, one for each height and one more for the non-height-divided image). Finally, to avoid border fading effects, eroded images are also correlated for each sector and height (15+5+4 more track vectors). As a result, 48 cross correlation vectors are computed from the 3 raster images.

Each vector is calculated as the average shown in the Equation (2).

$$V = \frac{v_{1-2} + v_{2-3}}{2} \tag{2}$$

if it is accomplished the sentences give by the Equation (3):

$$
\begin{aligned}
\left\| |v_{1-2}| - |v_{2-3}| \right\| &\leq 10 ms^{-1} \\
|\varphi_{1-2} - \varphi_{2-3}| &\leq 20° \\
\left\| |2V| - |v_{1-3}| \right\| &\leq 20 ms^{-1} \\
|\varphi - \varphi_{1-3}| &\leq 40°
\end{aligned}
\tag{3}
$$

where φi-j is the angle between vectors i and j, or if vectors are small enough:

$$
\begin{aligned}
|v_{1-2}| &\leq 10 ms^{-1} \\
|v_{2-3}| &\leq 10 ms^{-1} \\
|v_{1-3}| &\leq 10 ms^{-1} \\
|V| &\leq 10 ms^{-1}
\end{aligned}
\tag{4}
$$

without considering their phase φ. If v1-2, v2-3 and v1-3 satisfy Eqs. (3) or (4), then V is a coherent vector. If they do not, then a error code is assigned to V. Once the 48 vectors are flagged as coherent or filled with error codes, six quality tests are applied over them to choose the proper cloud tracking vector for each height and sector.

- First test deletes erroneous vectors. If vectors from eroded images of a particular height are equal to zero for the five sectors, vectors from non-eroded images are considered invalid.
- Then, if vector from the non-eroded image is invalid and the corresponding one from the eroded image is not, the last one is taken as the proper cloud vector.
- If vectors from eroded and non-eroded images differ by more than 20 m s^{-1} modulus or 40º phase, both are considered invalid vectors.
- If no valid vector is available for a particular sector and a particular height, vector from the entire image correlation of the same height is chosen as the proper vector for this sector.
- If there is no spatial coherence (considering both modulus and phase) between vectors from different sectors of the same height, vector from entire image at the same height is chosen as proper vector for the different sector or sectors. There should be at least three coherent sectors.
- If a vector from the entire image is not valid, vector from the non-height-divided image is taken for the needed sector.

At last, if no vector could be used for a particular sector and height, the last one from the previous cloud track determination is used.

3. Results

Results from cloud detection, opaque cloud tagging and cloud tracking are detailed in this section.

3.1 Cloud detection

A total of 795 MSG satellite images have been processed and clouds have been detected by the algorithm described. These images correspond to April, July and October of 2010. In parallel, images from TSI-880 camera have been analyzed. By visual inspection, TSI-880 images have been classified into three groups: cloudless sky, overcast and partially cloudy. Meanwhile, cloud detection results are saved automatically for several frame sizes centered at the University of Almería. These frame sizes vary from 5x7 to 13x17 pixels. Considering an average pixel size of 4.2x3 km^2, frames cover from 21x21 to 54.6x51 km^2. Different frame sizes are needed due to the whole-sky camera horizon uncertainty. Cloudy pixels on the frame are compared with total number of pixels and situations are also divided into three categories: cloudless, if the number of cloudy pixels is below 1/8 of the total pixel amount; overcast if it is over 7/8, and partially cloudy otherwise.

Comparing cloud cover situations, agreement in sky cover type could be used as agreement in cloud detection. Comparison between the whole-sky camera and satellite imagery could lead to wrong conclusions due to the following causes, all related to cameras hemispherical geometry: camera's horizon (high clouds appear sooner in whole sky images than low clouds at the same distance, whereas height does not affect satellite imagery). Camera's oktas determination (a small low cloud could fill more scene than a big high cloud whereas cloud size is not relative to the height in satellite images). Cloud visual transparency (high semitransparent cirrus could be undetected in the visual inspection whereas they are supposed to be detected by the test algorithm). Multiple cloud layers (contrast in whole-sky camera may lead to a sky misclassification). Figure 2 shows coincidence percentage between both visual and automatic sky classifications for a 9x11 pixel frame centered at the University of Almería. It is worth pointing out that cloud detection algorithm always detects

clouds in overcast situations (0% of MSG cloudless and TSI-880 overcast) and never fills the frame with clouds in cloudless situations (0% of MSG overcast and TSI-880 cloudless).
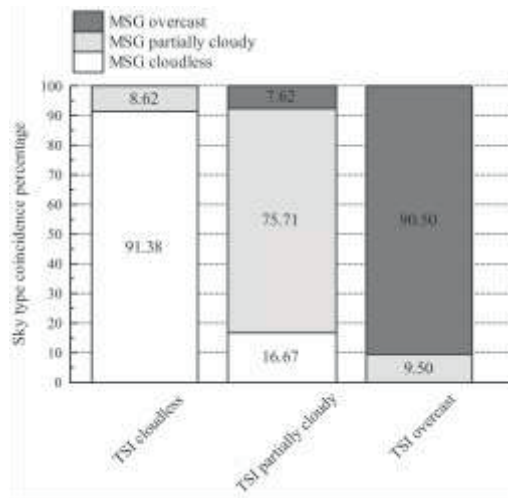

Fig. 2. Percentage of correct sky type situation for a 9x11 frame pixel size

Cloudless and overcast skies are well identified by detection algorithm as there is more than a 90% of agreement with visual classification in both situations. Partially cloudy skies show a 75% of coincidence percentage.

Figure 3 shows sky type coincidence percentage for different frame sizes. As the frame gets bigger, more clouds can enter it and cloudy pixel rate can become higher than 1/8, reaching the partially cloudy oktas interval. Thus, distant high clouds can appear on the whole-sky camera but in a small frame, this is why partially cloudy type may become better for larger frames.
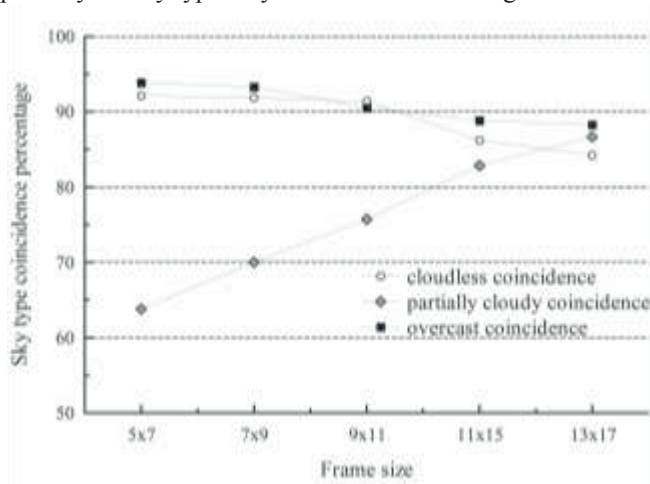

Fig. 3. Sky type coincidence percentage for several frame sizes. VIS, IR, NIR/VIS, T-T and ST stand for visible, infrared, ratio, difference and spatial texture test detection respectively. Op stands for the opaque pixel test proposed by Derrien and Le Gléau (2010) [18], which shows uniformly covered pixels from non-uniformly covered pixels. L, M and H stand for low, medium and high cloud top height, respectively.

3.2 Opaque cloud tagging

Figure 4 shows the percentage of detection test results in cases where direct irradiance is over and below 400 W m^{-2}.
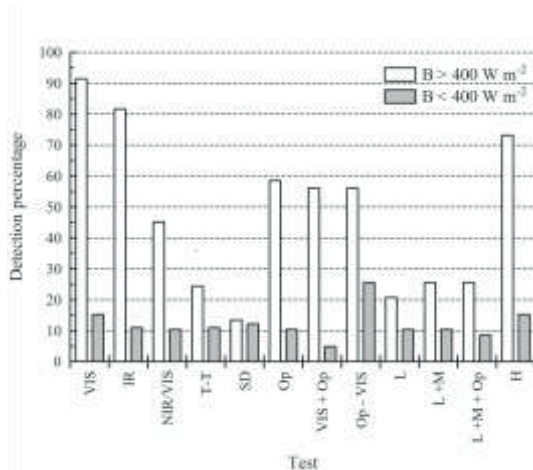

Fig. 4. Different detection test percentage

It can be seen that the visible test detects 91.5% of opaque clouds. A 15.2% of pixel situations when beam radiation exceeds 400 W m^{-2} is also detected by this test. Although there is a high misclassification rate, opaque clouds over-detection is preferable for power plant operation warnings. In addition, many of these situations could be caused by small or broken cumulus clouds that may allow beam radiation to reach ground between their empty spaces or holes.

3.3 Cloud tracking

A total of 11250 estimated vectors have been calculated for the cloud tracking method evaluation. They correspond to 120 days of 5 different months, January, February, April, July and October of 2010, from 0900 to 1500 UTC. Visual check on consecutive satellite processed images and TSI-880 pictures has been made to verify resulting vectors at different heights and in different sectors. Three kinds of error may be found: modulus error, phase error or rejected vector by quality tests. These rejected vectors are considered errors because the inability of the method to provide a motion vector while cloud motion is observed. Figure 5 shows checked errors pie graph.
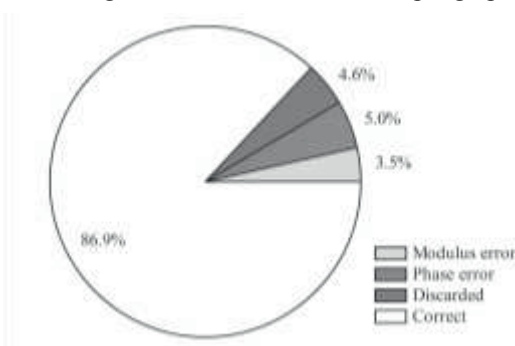

Fig. 5. Average error pie

Cloud tracking error is therefore around 10%. Figure 6 analyzes the error contribution of different cloud heights. Low clouds, which usually are the most opaque, have a little contribution to the total error. Direction errors are the major contribution to the total error though they are mostly due to high clouds.
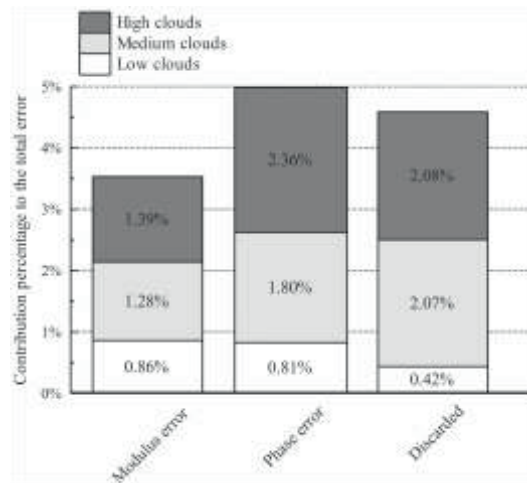

Fig. 6. Height error contribution

4. Conclusions

It has been pointed out that cloud detection, cloud classification and cloud motion determination are required for the forecast of cloud cover. These three tasks and short term cloud forecast could be solely performed by multispectral satellite imagery. Multispectral analysis is needed to detect clouds and classify them in terms of top height and opacity. Specifically, infrared channels are essential for cloud height assignment and visible channel is necessary for cloud opacity determination. It has been obvious that visible channels are remarkably important to detect thick clouds due to their high reflectance.

Cloud cover agreement has been used to infer cloud detection results.

To check detection results a whole-sky imager has been taken as reference. Results show an agreement above 90% between satellite detected and observed cloud cover for cloudless and overcast situations, and over 75% for partially cloudy skies.

Binary cross-correlation method has been chosen to estimate cloud motion vectors. Coherence and quality test over cloud motion vectors are quite significant. Results show that over 86% of the motion vectors are well determined. High clouds have a significant contribution to the error but many of them would not affect sun shading predictions as they are thin clouds with low opacity.

This work represents the starting point for addressing the prediction of solar radiation to short time using satellite imagery.

Acknowledgements

References

[1] Janjai S, Pankaew P, Laksanaboonsong J. A model for calculating hourly global solar radiation from satellite data in the tropics. Applied Energy 2009;86(9):1450-7.

[2] Şenkal O. Modeling of solar radiation using remote sensing and artificial neural network in turkey. Energy 2010;35:4795-801.

[3] Lu N, Qin J, Yang K, Sun J. A simple and e_cient algorithm to estimate daily global solar radiation from geostationary satellite data. Energy 2011;36:3179-88.

[4] Saunders RW. An automated scheme for the removal of cloud contamination from AVHRR radiances over western Europe. International Journal of Remote Sensing 1986;7(7):867-86.

[5] Saunders RW, Kriebel KT. An improved method for detecting clear sky and cloudy radiances from AVHRR data. International Journal of Remote Sensing 1988;9(1):123-50.

[6] Derrien M, Farki B, Harang L, LeGl_eau H, Noyalet A, Pochic D, et al. Automatic cloud detection applied to NOAA-11/AVHRR imagery. Remote Sensing of Environment 1993;46(3):246-67.

[7] Chen PY, Srinivasan R, Fedosejevs G, Narasimhan B. An automated cloud detection method for daily NOAA-14 AVHRR data for Texas, USA. International Journal of Remote Sensing 2002;23(15):2939-50.

[8] Thiermann V, Ruprecht E. A method for the detection of clouds using AVHRR infrared observations. International Journal of Remote Sensing 1992;13(10):1829-41.

[9] Amato U, Antoniadis A, Cuomo V, Cutillo L, Franzese M, Murino L, et al. Statistical cloud detection from SEVIRI multispectral images. Remote Sensing of Environment 2008;112(3):750-66.

[10] Ricciardelli E, Romano F, Cuomo V. Physical and statistical approaches for cloud identi_cation using Meteosat Second Generation-Spinning Enhanced Visible and Infrared Imager Data. Remote Sensing of Environment 2008;112(6):2741-60.

[11] Moussu G, Diabate L, Obrecht D, Wald L. A method for the mapping of the apparent ground brightness using visible images from geostationary satellites. International Journal of Remote Sensing 1989;10(7):1207-25.

[12] Nieman SJ, Schmetz J, Menzel WP. A comparison of several techniques to assign heights to cloud tracers. Journal of Applied Meteorology 1993;32(9):1559-68.

[13] Leese JA, Novak CS, Taylor VR. The determination of cloud pattern motions from geosynchronous satellite image data. Pattern Recognition 1970;2(4):279-92.

[14] Rutledge G, Legg E, Menzel P. Operational production of winds from cloud motions. Global and Planetary Change 1991;4(13):141-50.

[15] Laurent H. Wind extraction from meteosat water vapor channel image data. Journal of Applied Meteorology 1993;32(6):1124-33.

[16] Schmetz J, Holmlund K, Ho_man J, Strauss B, Mason B, Gaertner V, et al. Operational cloud-motion winds from Meteosat infrared images. Journal of Applied Meteorology 1993;32(7):1206-25.

[17] EUMETSAT. Effective radiance and brightness temperature relation for Meteosat 8 and 9. EUM/OPS/MSG/TEN/08/0024. Available online; 2009.

[18] Derrien M, Le Gléau H. Algorithm theoretical basis document for "Cloud products" (CMa-PGE01 v3.0, CT-PGE02 v2.0 & CTTH-PGE03 v2.1). Available online; 2010.

[19] Chen PY, Srinivasan R, Fedosejevs G, Narasimhan B. An automated cloud detection method for daily NOAA-14 AVHRR data for Texas, USA. International Journal of Remote Sensing 2002;23(15):2939-50.

[20] Derrien M, Le Gléau H. MSG/SEVIRI cloud mask and type from SAFNWC. International Journal of Remote Sensing 2005;26(21):4707-32.

[21] of Wyoming U. Department of Atmospheric Science; 2011. Http://weather.uwyo.edu/upperair/sounding.html.

[22] Stowe LL, Wellemeyer CG, Yeh HYM, Eck TF. Nimbus-7 global cloud climatology. part I: Algorithms and validation. Journal of Climate 1988;1(5):445-70.